A Revised Dosimetric Model of the Adult Head and Brain

Lionel G. Bouchet, Wesley E. Bolch, David A. Weber, Harold L. Atkins and John W. Poston, Sr.
Department of Nuclear Engineering, Texas A&M University, College Station, Texas; Department of Radiology, University of California, Davis, California; Department of Radiology, State University of New York, Stony Brook, New York

During the last decade, several new radiopharmaceuticals have been introduced for brain imaging. The marked differences of these tracers in tissue specificity within the brain and their increasing use for diagnostic studies support the need for a more anthropomorphic model of the human brain and head. Brain and head models developed in the past have comprised only simplistic representations of this anatomic region. **Methods:** A new brain model has been developed which includes eight subregions: the caudate nucleus, the cerebellum, the cerebral cortex, the lateral ventricles, the lentiform nucleus, the thalamus, the third ventricle and the white matter. This brain model has been included within a slightly modified version of the head model developed by Poston et al. in 1984. The head model, which includes both the thyroid and eyes, was modified in this work to include the cerebrospinal fluid within the cranial and spinal regions. **Results:** Absorbed fractions of energy for photon and electron sources located in thirteen source regions within the new head model were calculated using the EGS4 Monte Carlo radiation transport code for radiations in the energy range 10 keV to 4 MeV. **Conclusion:** S-values were calculated for five radionuclides used in brain imaging (^{11}C, ^{15}O, ^{18}F, ^{99m}Tc and ^{123}I) and for three radionuclides showing selective uptake in the thyroid (^{99m}Tc, ^{123}I, and ^{131}I). S-values were calculated using 100 discrete energy points in the beta-emission spectrum of the different radionuclides.

Key Words: internal dosimetry; brain and head dosimetry model; S-values

J Nucl Med 1996; 37:1226–1236

The estimation of absorbed dose in various organs from internal sources of photons or electrons is complicated by the complex structures and inhomogeneities of the various body organs. Consequently, simplified mathematical models of the human body have been developed based on three-dimensional geometrical descriptions of these organs. Previous models of the head and brain have been developed in a similar manner to support dosimetry studies of this body region. Nevertheless, they have remained simplistic representations of the head and brain, incorporating only minimal compartmentalization of functional or structural regional anatomy within the brain.

Radiopharmaceuticals used for brain imaging selectively localize in different structures of the brain, and thus, dosimetrically, it is important to have a model that closely resembles this organ (*1,2*). Consequently, a more detailed mathematical model of the brain and its subregions has been developed. This revised brain model is composed of eight regions: the caudate nucleus, the cerebellum, the cerebral cortex, the lateral ventricles, the lentiform nucleus (composed of the putamen and globus pallidus), the thalamus, the third ventricle and the white matter.

This model is incorporated into the Monte Carlo code EGS4 to calculate absorbed fractions and specific absorbed fractions of energy for both photon and electron sources in the energy range of 10 keV to 4 MeV. For each brain subregion considered as a source, a uniform distribution of photon and electron emissions is assumed. These calculations are performed using a revision of the head model developed by Poston et al. (*3*).

S-values are also calculated for several radionuclides. In this study, the beta particle component of the S-values is based on specific absorbed fractions evaluated at approximately 100 different energy values of the beta particle energy spectrum for each beta-emitting radionuclide. This technique should provide more accurate estimates of radionuclide S-values than those based only on the mean beta-particle energy. S-values for the brain subregions, the modeled regional structures and the cerebral spinal fluid are calculated for ^{11}C, ^{15}O, ^{18}F, ^{99m}Tc, and ^{123}I for the sources in the various subregions in the brain and in the cerebrospinal fluid of the spinal region. S-values are also calculated for ^{99m}Tc, ^{123}I, and ^{131}I for the thyroid as a source region.

REVIEW OF PREVIOUSLY PUBLISHED HEAD AND BRAIN MODELS

The first model of the brain and head for use in internal dose assessment was published in 1969 in MIRD Pamphlet No. 5, in which the brain was modeled as a single ellipsoid of soft tissue (*4*). The head and neck regions were represented by a simple truncated elliptical cylinder which enclosed the skull surrounding the brain, the spine and the thyroid. In 1978, a revision to Pamphlet No. 5 was issued in which the head was changed to be represented by a right elliptical cylinder topped by half an ellipsoid (*5*). In 1980, Cristy reported on the development of six mathematical phantoms representing children of various ages (*6*). In each phantom, the brain was again modeled as a single ellipsoid of soft tissue. In addition, a separate facial skeleton was added. In a separate study, Eckerman et al. (*6*) modified the adult brain model of Cristy to include a differentiation of the white and gray matter. A gray matter region was added, defined as an ellipsoidal shell with a slab dividing the brain into two hemispheres. Finally, Poston et al. (*3*) developed a new model of the head and brain in 1984 in which 14 regions of the head were identified. A differentiation between gray and white matter was also made in this model. Portions of this model are used in the present study.

Received Jun. 26, 1995; revision accepted Oct. 8, 1995.
For correspondence or reprints contact: Wesley E. Bolch, PhD, University of Florida, P.O. Box 118300, 202 Nuclear Science Center, Gainesville, FL 32611-8300.

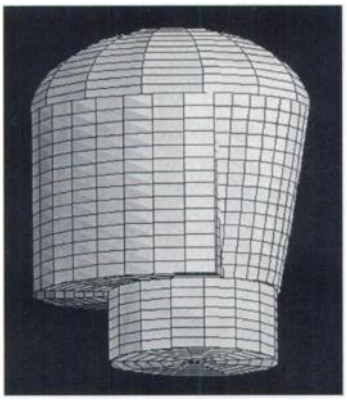

FIGURE 1. External features of the head and brain model.

A REVISED DOSIMETRIC MODEL FOR THE BRAIN AND HEAD

The shape of the head model is shown in Figure 1. Unlike previous head models, the neck and head are treated as two separate compartments. The neck is represented by a circular cylinder. It is topped by a cylindrical head region cut in the back by a cone, so that its bottom base coincides with the top of the neck. Two vertical planes on the back join the cone to the cylinder of the head. The top of the head is defined by a half ellipsoid. The trunk region of the Snyder-Fisher phantom without its internal organs (*4,5*) is incorporated into the model to take into account photons which could backscatter from the trunk into the head region.

Subregions within the Head

Twenty-one subregions are modeled within the head and neck region. A list of the subregions and their volumes is given in Table 1. The five regions representing bony structures contain a homogenized mixture of bone and red marrow with a density of 1.4 g cm^{-3}; the others are tissue regions with a density of 1.04 g cm^{-3} (the Cristy and Eckerman density values (*7*) are used for the both tissue and bone regions). Table 2 gives the composition of the tissue and bone regions.

Figure 2 shows a three-dimensional sagittal view of the new dosimetric model of the brain and head. Each modeled subregion is represented by a different color. The surrounding skin is not shown but is included in the model as a 2-mm thick region covering the entire head and neck. The thyroid is shown in red and the spinal region extends into the head. The thyroid is composed of two lobes. These two lobes are modeled as the volumes between two concentric cylinders cut by a fourth degree surface, two horizontal planes and one vertical plane. Its volume and shape are based upon ICRP Publication 23 (*9*). The spinal region is composed of three subregions: the spinal skeleton (a bone region shown in magenta), the spinal cerebrospinal fluid (CSF) shown in green, and the spinal column shown in pink. The spinal region represents a combination of the model of Poston et al. (*3*) and the one developed by Johansson and Nosslin (*10*) for the CSF in the spinal cord region and the region distal to the spinal cord. The three regions that compose the spinal region are modeled as cylinders bounded by the skull region at their top and by the base of the neck at their bottom.

In the front part of the head are located three bone regions: the mandible (gray), the teeth (maroon), and the upper face region (pink). The mandible is modeled as the volume between three elliptical cylinders cut by two planes: one plane is inclined to correspond to the cutting plane of the skull (maroon), and one vertical plane corresponds to the back of the teeth and upper face region. The teeth are represented by two concentric cylinders that fit between the mandible and the upper face region. Above the teeth is the upper face region defined as an elliptical cylinder bounded by the skull at the top and the mandible on the back. Inside the upper face region are two spherical eyes. The dimensions of all these regions are based upon data given in ICRP Publication 23 (*9*).

The skull (maroon) is defined as the volume between two concentric ellipsoids cut by two inclined planes. Within the skull is a 0.9-mm layer (green) that represents the subarachnoid space containing the CSF. These two regions are based on data given in ICRP Publication 23 (*9*) and Johansson and Nosslin (*10*).

TABLE 1
Regions and Their Corresponding Volumes within the Head and Brain Model

Region	Volume (cm^3)
Brain (total)	1467.6
Caudate nucleus	10.5
Cerebellum	139.1
Cerebral cortex	622.4
CSF in skull	56.9
Eyes	15.2
Head	4032.7
Lateral ventricles	20.1
Lentiform nucleus	19.4
Mandibles	170.5
Neck	567.4
Skin	280.1
Skull	364.6
Spinal column	6.8
Spinal CSF	14.9
Spinal skeleton	111.8
Teeth	31.2
Thalamus	6.0
Third ventricle	1.2
Thyroid	19.9
Upper face region	265.5
White matter	648.4

TABLE 2
Elemental Composition of the Soft Tissue and Bone Regions (*7*)

	Percent by weight	
Element	Soft tissue	Bone regions
H	10.454	7.337
C	22.663	25.475
N	2.490	3.057
O	63.525	47.893
F	0.000	0.025
Na	0.112	0.326
Mg	0.013	0.112
Si	0.030	0.002
P	0.134	5.095
S	0.204	0.173
Cl	0.133	0.143
K	0.208	0.153
Ca	0.024	10.190
Fe	0.005	0.008
Zn	0.003	0.005
Rb	0.001	0.002
Sr	0.000	0.003
Zr	0.001	0.000
Pb	0.000	0.001
Density	1.04 g cm^{-3}	1.4 g cm^{-3}

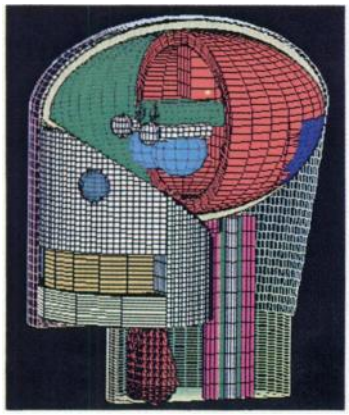

FIGURE 2. Interior features of the head and brain model.

Subregions within the Brain

The brain is located inside the skull and is surrounded by the CSF in the subarachnoid space. The current brain model includes eight subregions: the caudate nucleus, the cerebellum, the cerebral cortex, the lateral ventricles, the lentiform nucleus, the thalamus, the third ventricle, and the white matter. The revised brain model can be seen in Figure 2 inside the head model; a separate view is given in Figure 3. The shapes and volumes of the subregions of the brain were derived from volumes quoted in the literature (*11–14*) and from direct measurements taken from anatomical images of the head and brain (*15*).

The cerebral cortex (red) forms the shell of the brain and is defined by two half ellipsoids. The bottom ellipsoid is cut by both an inclined plane and by a vertical plane; the top ellipsoid is not cut. A constant 1-cm thickness is assigned, and at its center the cortex extends within the brain as a 1-cm thick parallelepiped. The cerebral cortex is cut on the back in a wedge-like fashion to accommodate the cerebellum (blue). A 1-cm thickness of the cerebral cortex also covers the two interior plane regions of the cerebellum. The volume of the model's cerebral cortex is 622.4 cm^3. Blinkov and Glezer (*11*) report that the ratio of the cerebral cortex volume to the of the total brain volume is ~44%. The ratio of volumes in the current model is 42.4%.

The cerebellum (blue) is located on the back of the brain. It is defined by an ellipsoid cut by one vertical plane and one horizontal plane. The two planes correspond to the layers of cerebral cortex covering the cerebellum. The cerebellum has a volume of 139.1 cm^3. ICRP Publication 23 (*9*) states that of the total brain volume, the cerebellum, comprises ~10%. In this model, the cerebellum comprises ~9.5% of the total brain volume.

The thalamus (yellow) is modeled as two ellipsoids which form the right and left thalamus. Its total volume is 6 cm^3 with each thalamus occupying 3 cm^3. Kurepina (*12*) reports a volume of 3.3 cm^3 for each thalamus.

The basal ganglia are separated into two parts: the caudate nucleus and the lentiform nucleus (the putamen plus the globus pallidus). The caudate nucleus (pink) is represented by two symmetrical cylinders, capped on one side by a sphere representing the head of the caudate nucleus. The total volume is 10.5 cm^3. Harman and Carpenter (*13*) report a volume of 10.5 cm^3 for the adult caudate nucleus. In a single hemisphere, one caudate nucleus is located between one lateral ventricle (green) and one lentiform nucleus (blue).

Based upon a review of the anatomy of the basal ganglia region, a decision was made to model each lentiform nucleus (blue) as a single ellipsoid (23.88 cm^3) less the intersecting volumes of the caudate nucleus and thalamus in the respective hemisphere. Consequently, the simulated volume of each lentiform nucleus is reduced to 19.2 cm^3. Harman and Carpenter report a volume of 19.3 cm^3 for this region (*13*).

The ventricles (green) of the brain have been separated into their various components. First, the third ventricle is located between the two thalami and is represented as an elliptical cylinder with a volume of 1.2 cm^3. The lateral ventricles are modeled as two right circular cylinders with a volume per ventricle of 10.1 cm^3. They are located just below the internal portion of the cerebral cortex. Thus, the total volume of the ventricles (lateral ventricles and third ventricle) is 21.3 cm^3. Tompsett and Last (*14*) report that 1.6% of the total brain volume is occupied by the ventricles thus giving a volume of 21.3 cm^3 considering the total brain volume of the model of 1467 cm^3.

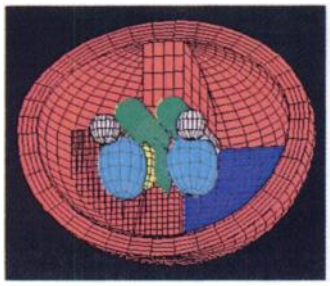

FIGURE 3. Interior features of the brain model.

ABSORBED FRACTION CALCULATIONS

Absorbed fractions of energy and specific absorbed fractions of energy for several particle energies, and for several source regions were calculated using the EGS4 Monte Carlo code (*16*). Twelve initial energies were chosen between 10 keV and 4 MeV for both photons and electrons. Thirteen sources were included: the eight brain subregions, the skull, the CSF in the skull, the spinal skeleton, the spinal CSF and the thyroid (*17*). Ten history sets of 100,000 particles were run for each source region and for each particle energy, for a total of 1,000,000 particles [10,000 particles were run for the data in MIRD Pamphlet No. 5 (*4*) and 60,000 for the data in MIRD Pamphlet No. 5 Revised (*5*)]. A Sun Sparcstation 20, Model 512 was used in this research. A simulation of 12,000,000 particles (1,000,000 particles per energy and 12 different energies considered) took approximately 10 CPU-hours for each photon source region, and 40 CPU-hours for each electron source region.

Calculations were performed for all source regions for both photons and electrons. The absorbed fraction and specific absorbed fraction were calculated for each region in the head model, plus the soft tissue region representing the trunk. Due to the large number of particles simulated, coefficients of variations of absorbed fractions values are typically less than 1% for absorbed fractions greater than 10^{-3} and less than 5% for absorbed fractions greater than 10^{-4} (*17*). Consequently, standard deviations are not visible on the figures described below.

Figure 4 displays a plot of the self absorbed fractions for various photon source regions located within the brain (a self-absorbed fraction is defined as the absorbed fraction for a region designated as both source and target). As expected, the absorbed fraction increases rapidly with decreasing photon energy below 100 keV primarily due to the rise in the linear attenuation coefficient for photoelectric absorption. The absorbed fraction of energy is larger for larger organs at all photon energies (the white matter is the largest region and has the largest self absorbed fraction, while the third ventricle is the smallest region and has the smallest absorbed fraction). The total soft-tissue volume of a region, however, is only a rough

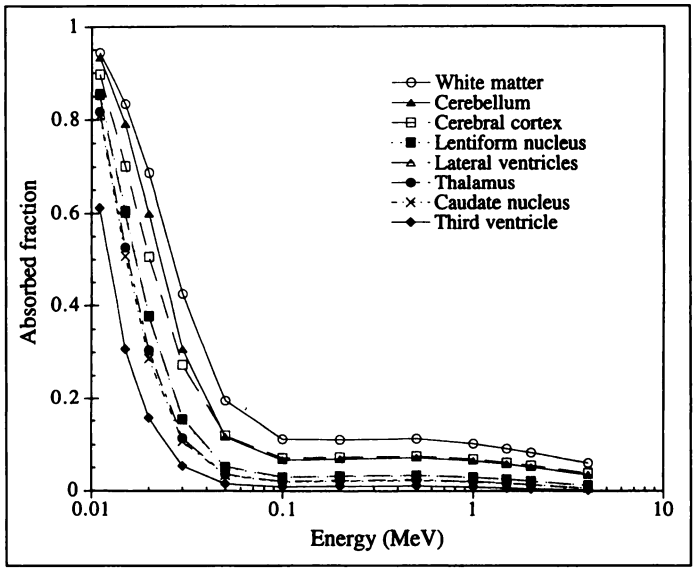

FIGURE 4. Self-absorbed fractions for photon sources located within the brain.

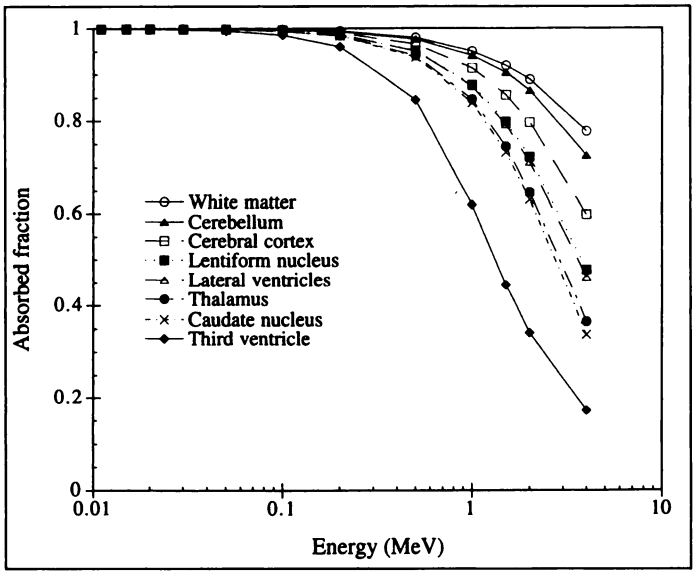

FIGURE 6. Self-absorbed fractions for electron sources located within the brain.

indicator of the relative magnitude of the photon self absorbed fraction. For example, the cerebellum and the cerebral cortex have tissue volumes of 139 cm^3 and 622 cm^3, respectively, and yet they have essentially equivalent absorbed fractions at photon energies greater than 50 keV. Moreover, the smaller tissue region of the cerebellum exhibits a higher self-absorbed fraction than that of the larger cerebral cortex at photon energies below 50 keV. This pattern at lower energies is due primarily to the larger surface-to-volume ratio of the cerebral cortex as compared to the cerebellum (the cerebral cortex is a convex region while the cerebellum is a concave region). Consequently, a randomly directed photon emitted in the cerebral cortex will have a greater opportunity to leave that region than if it had been emitted in the cerebellum, provided its mean-free-path is relatively small. As the mean-free-path increases with increasing photon energy above 50 keV, the influences of total tissue volume and the surface-to-volume ratio compensate one another yielding essentially equivalent values of the self absorbed fraction.

Figure 5 shows self-absorbed fractions of energy for the other regions of the improved head model. In this figure, the absorbed fractions for the two bone source regions (spinal skeleton and skull) are shown to be greater than for the soft-tissue and CSF regions. Bone regions have higher effective atomic numbers compared to the soft-tissue regions, and thus have larger linear attenuation coefficients than the soft-tissue regions. Furthermore, the Z dependence of the photon attenuation coefficient is greater at lower photon energies. Consequently, one observes a greater difference in absorbed fractions between bone and soft-tissue regions at photon energies below about 200 keV than at higher photon energies. In this figure, it also can be seen that the absorbed fraction depends on the surface-to-volume ratio. The spinal CSF is the smallest region, yet it does not exhibit the smallest absorbed fraction. In an argument similar to that made earlier, the absorbed fractions for the CSF within the skull are below those for the spinal CSF region at photon energies below about 50 keV primarily due to its larger surface-to-volume ratio.

In Figures 6 and 7, the self-absorbed fractions for electron sources are shown. The self-absorbed fraction for electron sources exhibits a different shape as a function of particle energy than for photon sources. At low energies, the self-absorbed fraction is very close to 1. The self-absorbed fraction

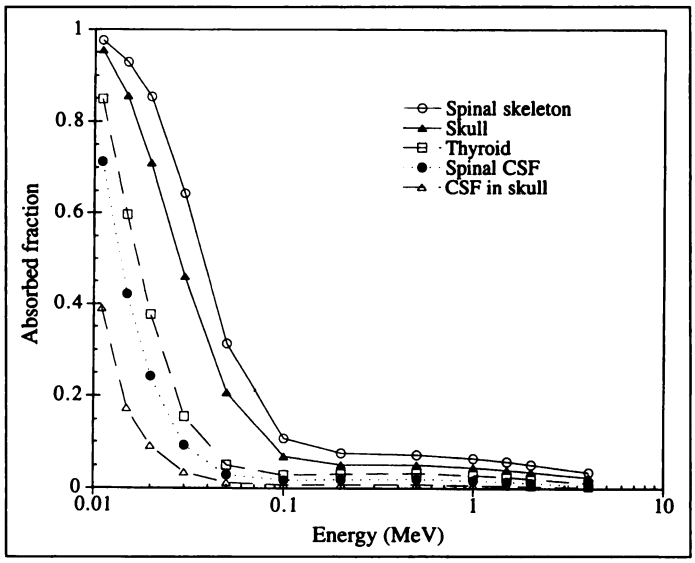

FIGURE 5. Self-absorbed fractions for photon sources located within the head (brain excluded).

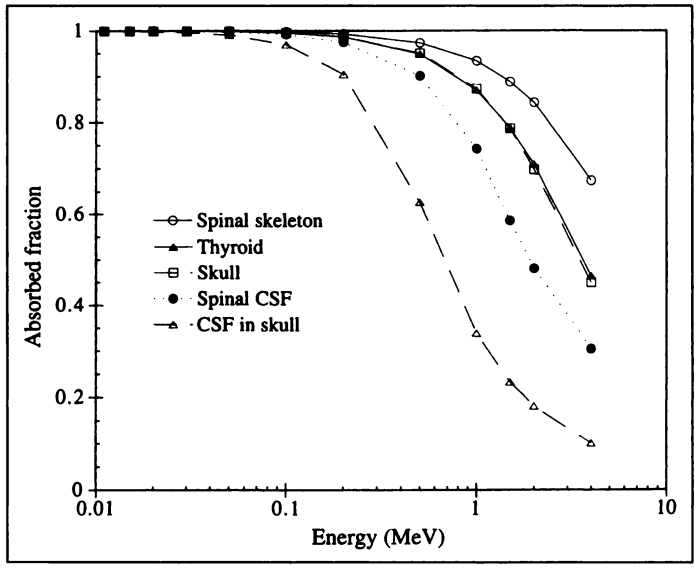

FIGURE 7. Self-absorbed fractions for electron sources located within the head (brain excluded).

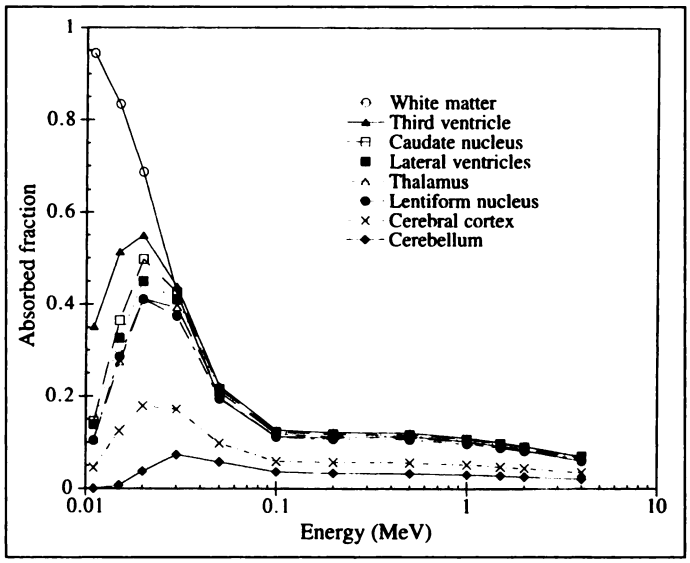

FIGURE 8. Absorbed fraction in the white matter for photon sources located in various regions within the brain.

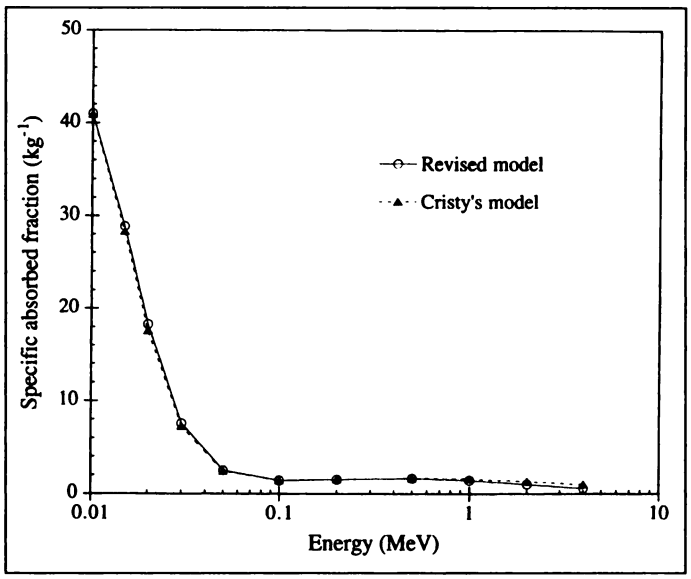

FIGURE 10. Comparison of the self-specific absorbed fraction of energy for the thyroid as a uniform source of monoenergetic photons for the current head and brain model and the Cristy head model (*7*).

then decreases with increasing electron energy. It can be seen that the decrease in the self-absorbed fraction with increasing particle energy depends on the volume of the region and also on the surface-to-volume ratio of the region. In Figure 6, the self-absorbed fraction in the cerebellum decreases less dramatically than that in the third ventricle. Figure 7 shows electron self-absorbed fractions in the head regions. Since the CSF region in the skull (56.9 cm^3) has a larger surface-to-volume ratio than the spinal CSF region (6.75 cm^3), its self-absorbed fraction is thus smaller than the self-absorbed fraction for the spinal CSF region even though it occupies a larger tissue volume.

Figure 8 shows the absorbed fraction of energy for the white matter as a target region and for various photon source regions within the brain. The shape of the absorbed fraction as a function of the energy is different if the source and the target are the same or are different. For different source and target regions, the absorbed fraction initially increases, then reaches a maximum and finally decreases with increasing photon energy. For source regions completely surrounded by the white matter, the smaller the source organ, the greater the absorbed fraction of energy in the white matter region. The two regions contributing the lowest values of absorbed fraction to the white matter are the cerebral cortex and the cerebellum, both of which lose an appreciable number of escaping photons to the surrounding skull region due to their geometrical arrangement within the brain.

Figure 9 shows the absorbed fraction of energy in the white matter as a target region and for various source regions of electrons within the brain. The absorbed fraction continually increases with increasing electron energy when the source does not equal the target. Again, electrons have shorter ranges at lower energies and thus their kinetic energy will principally be deposited in the source region. At higher energies, the electron range increases, allowing a greater fraction to escape the source region and contribute to the energy deposition in the surrounding regions.

CALCULATION OF S-VALUES

Specific absorbed fractions were used to calculate S-values for several radionuclides and several source regions of interest

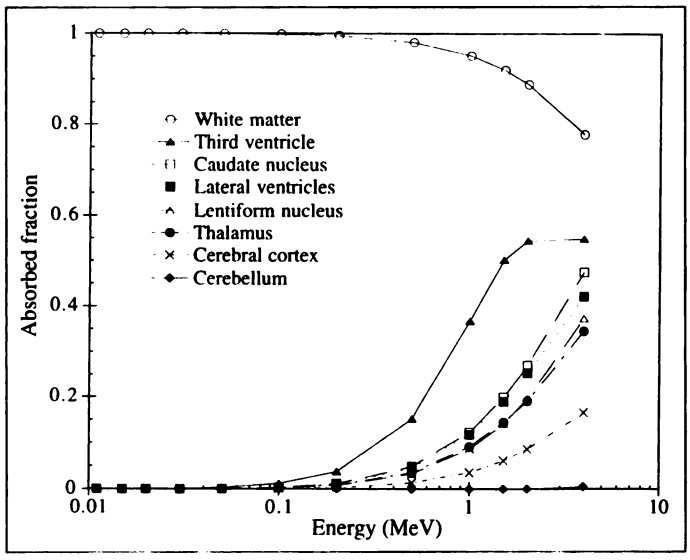

FIGURE 9. Absorbed fraction in the white matter for electron sources located in various regions within the brain.

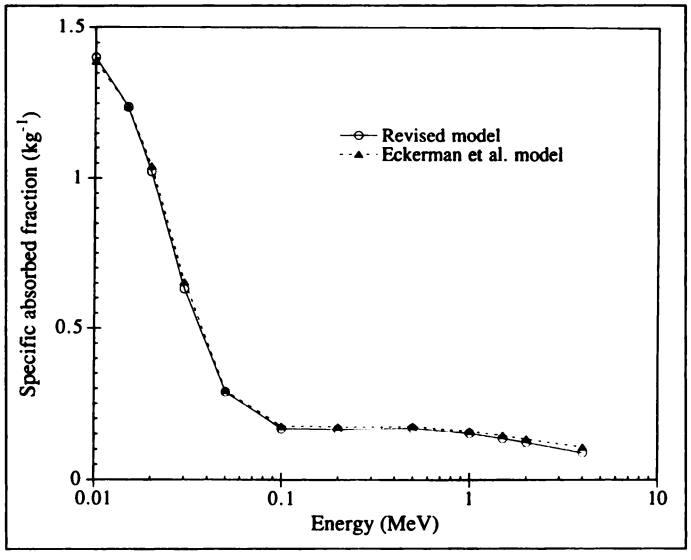

FIGURE 11. Comparison of the self-specific absorbed fraction of energy for the white matter region as a uniform source of monoenergetic photons for the current head and brain model and the brain model of Eckerman et al. (*8*).

in brain imaging (*17*). For beta-emitting radionuclides, a full beta-particle energy spectrum was used in the calculations. For each energy in the beta spectrum, a semilogarithmic interpolation of the specific absorbed fraction at this energy was made between the two closest energy points where the specific absorbed fraction has been calculated using the EGS4 program. For energies less than 10 keV, a linear extrapolation was performed between 0 and 10 keV. For this purpose, the absorbed fraction at zero keV was taken as unity for the source region and zero for the remaining target regions.

In this research, it was assumed that the electron transport results can be used to approximate S-values for positron-emitting radionuclides. The two annihilation photons were added in the calculations of the S-values as if a uniform distribution of 0.511 MeV photons originated in the source region. Nevertheless, explicit positron calculations should be made to take into account the track-length displacement of the annihilation events both inside and outside the source region. For high-energy positrons with ranges exceeding the dimensions of the source regions, explicit treatment of the annihilation events may result in slight differences in the values reported here.

S-values have been calculated for all the sources in the brain and for the CSF in the skull and spine for several radionuclides used in brain imaging. The results are presented in Appendix Tables A1 to A10 for the following radionuclides: ^{11}C, ^{15}O, ^{18}F, ^{99m}Tc and ^{123}I. Table A11 gives S values for the thyroid as a source region for the radionuclides ^{99m}Tc, ^{123}I and ^{131}I. S values calculations for some 32 additional radionuclides, and for additional source/target regions can be found in reference (*17*).

COMPARISONS WITH OTHER MODELS

A comparison of the specific absorbed fractions obtained in this research for the thyroid as a uniform source of photons can be made with the 1987 calculations of Cristy and Eckerman (*7*). Their thyroid model has the same shape as the current model presented here. Figure 10 displays the self-specific absorbed fraction of energy for the thyroid as a uniform source of photons. The two curves match very well up to a photon energy of 0.5 MeV, with the difference between the two calculations never exceeding 2%. Above 0.5 MeV, the difference between the two sets of values increases to 40% at 4 MeV. This larger difference at high photon energies results from the fact that the new calculations include electron transport with photon sources. In the Cristy and Eckerman calculations, only photons were transported and electrons were not considered.

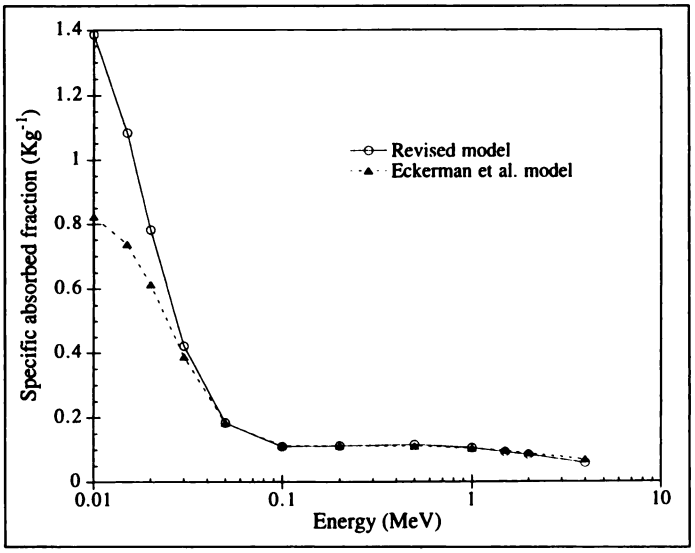

FIGURE 13. Comparison of the self-specific absorbed fraction of energy for the gray region as a uniform source of monoenergetic photons for the current head and brain model and the brain model of Eckerman et al. (*8*).

Other comparisons can be made with the calculations performed in 1980 by Eckerman, Cristy and Warner on their revised brain model (*8*) positioned within the Cristy head model (*6*). Their model includes a purely white matter region (189 cm^3) and a region composed of a mixture of gray and white matter (1178 cm^3). They calculated the specific absorbed fractions of energy for the total white matter volume (697 cm^3) and the total gray matter volume (669 cm^3) as both source and target regions. Figure 11 shows the specific absorbed fractions to the white matter for the white matter region as a uniform source of photons. The difference between the two calculated specific absorbed fractions is small for low to intermediate energy photons (less than 5% up to 1 MeV) and somewhat larger for high energy photons (a 20% difference is seen at 4

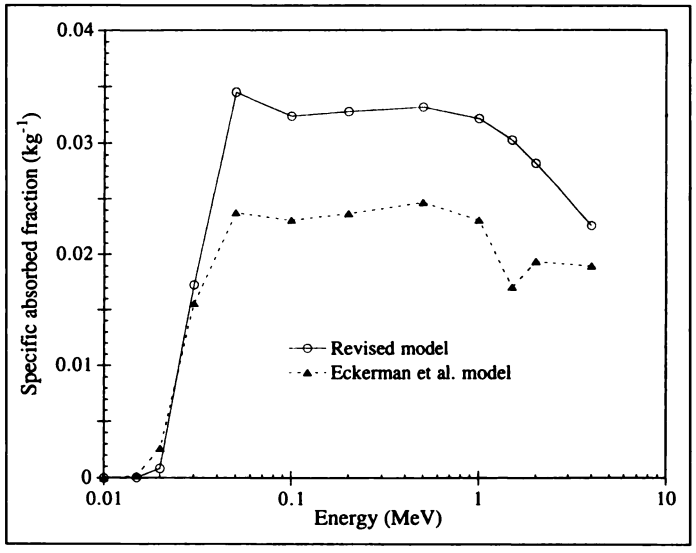

FIGURE 12. Comparison of the specific absorbed fraction of energy to the eyes for the white matter region as a uniform source of monoenergetic photons for the current head and brain model and the brain model of Eckerman et al. (*8*).

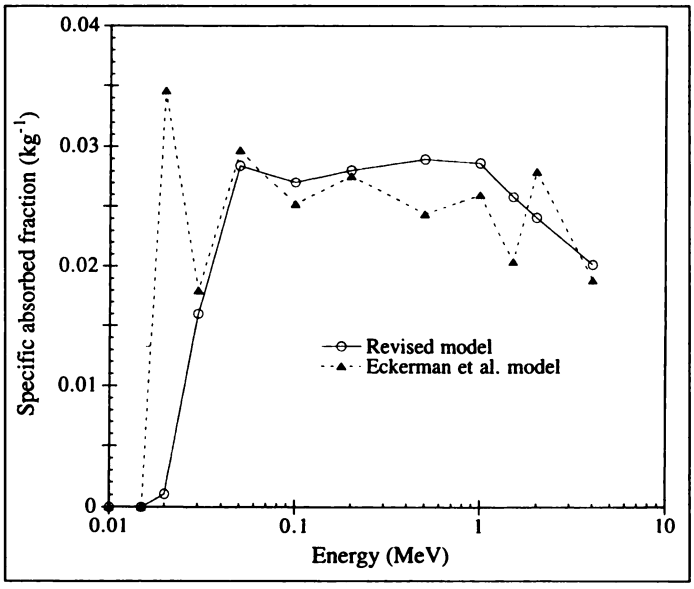

FIGURE 14. Comparison of the specific absorbed fraction of energy to the eyes for the gray region as a uniform source of monoenergetic photons for the current head and brain model and the brain model of Eckerman et al. (*8*).

MeV). Figure 12 compares the specific absorbed fraction to the eyes for the white matter region as a source of photons. The large difference shown is primarily due to differences in the model geometries. The new data provide a smoother representation of the energy dependence of this quantity due to the greater number of photons transported and the resulting lower coefficients of variation in these calculations.

Figure 13 shows the specific absorbed fraction to the gray matter for the gray matter region as a source of photons. The values show large differences for low energy photons (40% at 10 keV). The differences decrease to less than 10% in the energy range 30 keV to 2 MeV, then increase to 20% at 4 MeV. Figure 14 shows the specific absorbed fraction to the eyes for the gray matter region as a source of photons. Again, a smoother representation is found in the data generated in this research primarily due to the larger number of photons transported.

CONCLUSION

A new brain model has been developed primarily by measuring distances in the anatomic brain images as reported by Murtagh and Schintzlein (*15*). In addition, the volumes of each brain subregion have been kept as close as possible as to those reported in the literature (*11–14*). Eight subregions have been included: the caudate nucleus, the cerebellum, the cerebral cortex, the lateral ventricles, the lentiform nucleus, the thalamus, the third ventricle and the white matter. The outer shape of the brain has been kept the same as the outer shape of the brain model defined in the head model of Poston et al. (*3*).

This revised brain model has been included in the head model of Poston et al. (*3*). However, corrections have been made to some of the equations and volumes reported in this earlier reference. Furthermore, the spinal region was changed in order to include the cerebrospinal fluid. In addition, a thin layer of cerebrospinal fluid was added between the cranium region and the brain (subarachnoid space). The spinal region was also modeled in three parts: the spinal column, the spinal cerebrospinal fluid and the spinal skeleton.

This revised head model was used as the set of geometry routines in the EGS4 Monte Carlo code (*16*) to calculate absorbed fractions and specific absorbed fractions of energy for electron and photon sources. For this purpose, twelve energies were taken between 10 keV and 4 MeV based on previous calculations made by the MIRD Committee (*4,5*). Thirteen source regions have been used, including the eight brain subregions, cerebrospinal fluid in the skull, spinal cerebrospinal fluid, the skull, the spinal skeleton and the thyroid. One million histories were followed for each energy and for each source region for photon and electron sources.

S-values were calculated for five radionuclides (^{11}C, ^{15}O, ^{18}F, ^{99m}Tc, and ^{123}I) used in brain imaging and for three radionuclides (^{99m}Tc, ^{123}I, and ^{131}I) used in thyroid imaging. These S-values were calculated using discrete energy points describing the beta spectrum for each beta-particle emitter. These S-values can be used to calculate the absorbed dose to a given head or brain region for a given source region and a given radiopharmaceutical.

The development of improved head and brain models for the pediatric phantoms is also necessary. Cristy and Eckerman developed pediatric whole-body phantoms for a newborn, a 1-yr-old, a 5-yr-old, a 10-yr-old, a 15-yr-old (corresponding also to an adult female), and an adult male (*6*). However, the head and brain models for the various phantoms are given in the same level of detail as for the adult phantom. As one looks at these smaller phantoms, the MIRD Committee's traditional assumption of full electron energy deposition in the source region becomes less applicable. Consequently, if realistic dosimetric information in brain imaging is needed in pediatric nuclear medicine studies, similar developments in improved head and brain phantoms should be focused on obtaining accurate estimates of subregion volumes at these younger ages.

APPENDIX

TABLE A1
S-Values for Listed Radionuclides with the Caudate Nucleus as a Source Region

Targets	S-value (mGy MBq^{-1} s^{-1})				
	^{11}C	^{15}O	^{18}F	^{99m}Tc	^{123}I
Caudate nucleus	5.79×10^{-3}	9.76×10^{-3}	4.02×10^{-3}	2.79×10^{-4}	5.10×10^{-4}
Cerebellum	5.37×10^{-6}	5.39×10^{-6}	5.38×10^{-6}	7.27×10^{-7}	9.92×10^{-7}
Cerebral cortex	1.08×10^{-5}	1.09×10^{-5}	1.08×10^{-5}	1.43×10^{-6}	2.19×10^{-6}
Eyes	7.45×10^{-6}	7.48×10^{-6}	7.47×10^{-6}	8.89×10^{-7}	1.13×10^{-6}
Lentiform nucleus	1.23×10^{-4}	2.53×10^{-4}	9.65×10^{-5}	1.06×10^{-5}	2.10×10^{-5}
Skin in head	3.61×10^{-6}	3.62×10^{-6}	3.62×10^{-6}	4.01×10^{-7}	5.27×10^{-7}
Skin in neck	8.32×10^{-7}	8.35×10^{-7}	8.34×10^{-7}	7.36×10^{-8}	9.37×10^{-8}
Skull	7.11×10^{-6}	7.14×10^{-6}	7.12×10^{-6}	1.43×10^{-6}	2.24×10^{-6}
Spinal column	1.01×10^{-6}	1.01×10^{-6}	1.01×10^{-6}	1.28×10^{-7}	1.59×10^{-7}
Spinal skeleton	2.34×10^{-6}	2.35×10^{-6}	2.34×10^{-6}	4.83×10^{-7}	5.39×10^{-7}
Thalamus	6.40×10^{-5}	6.93×10^{-5}	6.40×10^{-5}	8.16×10^{-6}	1.56×10^{-5}
Thyroid	1.13×10^{-6}	1.14×10^{-6}	1.13×10^{-6}	1.29×10^{-7}	1.60×10^{-7}
White matter	3.36×10^{-5}	4.98×10^{-5}	3.04×10^{-5}	3.74×10^{-6}	6.73×10^{-6}

TABLE A2
S-Values for Listed Radionuclides with Cerebellum as a Source Region

Targets	S-value (mGy MBq^{-1} s^{-1})				
	^{11}C	^{15}O	^{18}F	^{99m}Tc	^{123}I
Caudate nucleus	5.04×10^{-6}	5.06×10^{-6}	5.05×10^{-6}	7.49×10^{-7}	1.01×10^{-6}
Cerebellum	5.13×10^{-4}	8.76×10^{-4}	3.66×10^{-4}	2.81×10^{-5}	5.22×10^{-5}
Cerebral cortex	1.25×10^{-5}	1.64×10^{-5}	1.17×10^{-5}	1.42×10^{-6}	2.41×10^{-6}
Eyes	1.21×10^{-6}	1.21×10^{-6}	1.21×10^{-6}	1.25×10^{-7}	1.50×10^{-7}
Lentiform nucleus	6.09×10^{-6}	6.11×10^{-6}	6.10×10^{-6}	8.67×10^{-7}	1.19×10^{-6}
Skin in head	4.61×10^{-6}	4.63×10^{-6}	4.62×10^{-6}	5.10×10^{-7}	7.24×10^{-7}
Skin in neck	9.43×10^{-7}	9.47×10^{-7}	9.45×10^{-7}	8.14×10^{-8}	1.05×10^{-7}
Skull	1.01×10^{-5}	1.22×10^{-5}	9.87×10^{-6}	1.77×10^{-6}	3.58×10^{-6}
Spinal column	1.74×10^{-6}	1.75×10^{-6}	1.75×10^{-6}	2.28×10^{-7}	2.88×10^{-7}
Spinal skeleton	3.96×10^{-6}	3.97×10^{-6}	3.96×10^{-6}	7.46×10^{-7}	9.02×10^{-7}
Thalamus	9.00×10^{-6}	9.03×10^{-6}	9.01×10^{-6}	1.20×10^{-6}	1.73×10^{-6}
Thyroid	9.16×10^{-7}	9.18×10^{-7}	9.18×10^{-7}	8.59×10^{-8}	1.07×10^{-7}
White matter	7.91×10^{-6}	7.94×10^{-6}	7.92×10^{-6}	1.04×10^{-6}	1.58×10^{-6}

TABLE A3
S-Values for Listed Radionuclides with Cerebral Cortex as Source Region

Targets	S-value (mGy MBq^{-1} s^{-1})				
	^{11}C	^{15}O	^{18}F	^{99m}Tc	^{123}I
Caudate nucleus	1.06×10^{-5}	1.07×10^{-5}	1.06×10^{-5}	1.44×10^{-6}	2.16×10^{-6}
Cerebellum	1.23×10^{-5}	1.63×10^{-5}	1.16×10^{-5}	1.43×10^{-6}	2.41×10^{-6}
Cerebral cortex	1.14×10^{-4}	1.92×10^{-4}	8.23×10^{-5}	6.39×10^{-6}	1.16×10^{-5}
Eyes	4.73×10^{-6}	4.75×10^{-6}	4.74×10^{-6}	5.52×10^{-7}	7.12×10^{-7}
Lentiform nucleus	1.10×10^{-5}	1.10×10^{-5}	1.10×10^{-5}	1.44×10^{-6}	2.23×10^{-6}
Skin in head	4.83×10^{-6}	4.85×10^{-6}	4.84×10^{-6}	5.24×10^{-7}	7.49×10^{-7}
Skin in neck	7.30×10^{-7}	7.33×10^{-7}	7.32×10^{-7}	6.27×10^{-8}	8.08×10^{-8}
Skull	1.07×10^{-5}	1.41×10^{-5}	1.04×10^{-5}	1.81×10^{-6}	3.79×10^{-6}
Spinal column	1.15×10^{-6}	1.15×10^{-6}	1.15×10^{-6}	1.51×10^{-7}	1.89×10^{-7}
Spinal skeleton	2.49×10^{-6}	2.50×10^{-6}	2.49×10^{-6}	4.74×10^{-7}	5.78×10^{-7}
Thalamus	1.07×10^{-5}	1.08×10^{-5}	1.07×10^{-5}	1.46×10^{-6}	2.19×10^{-6}
Thyroid	9.29×10^{-7}	9.31×10^{-7}	9.31×10^{-7}	9.05×10^{-8}	1.14×10^{-7}
White matter	1.53×10^{-5}	2.02×10^{-5}	1.43×10^{-5}	1.78×10^{-6}	3.02×10^{-6}

TABLE A4
S-Values for Listed Radionuclides with CSF in Skull as Source Region

Targets	S-value (mGy MBq^{-1} s^{-1})				
	^{11}C	^{15}O	^{18}F	^{99m}Tc	^{123}I
Caudate nucleus	8.20×10^{-6}	8.20×10^{-6}	8.18×10^{-6}	1.04×10^{-6}	1.54×10^{-6}
Cerebellum	2.25×10^{-5}	4.41×10^{-5}	1.64×10^{-5}	1.58×10^{-6}	2.75×10^{-6}
Cerebral cortex	2.90×10^{-5}	6.09×10^{-5}	1.99×10^{-5}	1.70×10^{-6}	3.04×10^{-6}
Eyes	5.07×10^{-6}	5.09×10^{-6}	5.08×10^{-6}	5.69×10^{-7}	7.39×10^{-7}
Lentiform nucleus	8.41×10^{-6}	8.44×10^{-6}	8.43×10^{-6}	1.12×10^{-6}	1.66×10^{-6}
Skin in head	5.68×10^{-6}	5.71×10^{-6}	5.70×10^{-6}	5.95×10^{-7}	8.67×10^{-7}
Skin in neck	7.34×10^{-7}	7.36×10^{-7}	7.36×10^{-7}	6.38×10^{-8}	8.23×10^{-8}
Skull	3.77×10^{-5}	8.55×10^{-5}	2.41×10^{-5}	2.49×10^{-6}	5.72×10^{-6}
Spinal column	1.28×10^{-6}	1.29×10^{-6}	1.29×10^{-6}	1.46×10^{-7}	1.91×10^{-7}
Spinal skeleton	2.84×10^{-6}	2.86×10^{-6}	2.85×10^{-6}	5.19×10^{-7}	6.47×10^{-7}
Thalamus	8.01×10^{-6}	8.05×10^{-6}	8.03×10^{-6}	1.07×10^{-6}	1.52×10^{-6}
Thyroid	9.15×10^{-7}	9.17×10^{-7}	9.17×10^{-7}	1.01×10^{-7}	1.22×10^{-7}
White matter	9.31×10^{-6}	9.34×10^{-6}	9.32×10^{-6}	1.19×10^{-6}	1.88×10^{-6}

TABLE A5
S-Values for Listed Radionuclides with Lateral Ventricles as Source Region

Targets	S-value (mGy MBq^{-1} s^{-1})				
	^{11}C	^{15}O	^{18}F	^{99m}Tc	^{123}I
Caudate nucleus	6.74×10^{-5}	9.67×10^{-5}	6.46×10^{-5}	8.30×10^{-6}	1.61×10^{-5}
Cerebellum	8.81×10^{-6}	8.84×10^{-6}	8.82×10^{-6}	1.18×10^{-6}	1.72×10^{-6}
Cerebral cortex	1.30×10^{-5}	1.32×10^{-5}	1.30×10^{-5}	1.72×10^{-6}	2.73×10^{-6}
Eyes	4.35×10^{-6}	4.36×10^{-6}	4.36×10^{-6}	4.99×10^{-7}	6.19×10^{-7}
Lentiform nucleus	4.28×10^{-5}	4.67×10^{-5}	4.25×10^{-5}	5.51×10^{-6}	1.00×10^{-5}
Skin in head	3.58×10^{-6}	3.59×10^{-6}	3.59×10^{-6}	4.05×10^{-7}	5.34×10^{-7}
Skin in neck	7.48×10^{-7}	7.51×10^{-7}	7.49×10^{-7}	6.99×10^{-8}	8.84×10^{-8}
Skull	6.79×10^{-6}	6.83×10^{-6}	6.80×10^{-6}	1.39×10^{-6}	2.07×10^{-6}
Spinal column	1.01×10^{-6}	1.02×10^{-6}	1.02×10^{-6}	1.34×10^{-7}	1.60×10^{-7}
Spinal skeleton	2.39×10^{-6}	2.40×10^{-6}	2.40×10^{-6}	4.89×10^{-7}	5.54×10^{-7}
Thalamus	7.41×10^{-5}	8.99×10^{-5}	7.24×10^{-5}	9.27×10^{-6}	1.79×10^{-5}
Thyroid	9.22×10^{-7}	9.25×10^{-7}	9.24×10^{-7}	1.01×10^{-7}	1.24×10^{-7}
White matter	3.28×10^{-5}	4.83×10^{-5}	2.97×10^{-5}	3.69×10^{-6}	6.56×10^{-6}

TABLE A6
S-Values for Listed Radionuclides with Lentiform Nucleus as Source Region

Targets	S-value (mGy MBq^{-1} s^{-1})				
	^{11}C	^{15}O	^{18}F	^{99m}Tc	^{123}I
Caudate nucleus	1.23×10^{-4}	2.53×10^{-4}	9.72×10^{-5}	1.06×10^{-5}	2.09×10^{-5}
Cerebellum	6.37×10^{-6}	6.39×10^{-6}	6.38×10^{-6}	8.61×10^{-7}	1.19×10^{-6}
Cerebral cortex	1.07×10^{-5}	1.08×10^{-5}	1.08×10^{-5}	1.44×10^{-6}	2.21×10^{-6}
Eyes	6.82×10^{-6}	6.84×10^{-6}	6.83×10^{-6}	8.14×10^{-7}	1.01×10^{-6}
Lentiform nucleus	3.27×10^{-3}	5.59×10^{-3}	2.27×10^{-3}	1.26×10^{-4}	2.34×10^{-4}
Skin in head	3.50×10^{-6}	3.51×10^{-6}	3.51×10^{-6}	3.86×10^{-7}	4.97×10^{-7}
Skin in neck	1.12×10^{-6}	1.12×10^{-6}	1.12×10^{-6}	1.17×10^{-7}	1.49×10^{-7}
Skull	7.48×10^{-6}	7.52×10^{-6}	7.49×10^{-6}	1.52×10^{-6}	2.43×10^{-6}
Spinal column	1.57×10^{-6}	1.58×10^{-6}	1.58×10^{-6}	1.93×10^{-7}	2.37×10^{-7}
Spinal skeleton	3.46×10^{-6}	3.48×10^{-6}	3.47×10^{-6}	7.33×10^{-7}	8.45×10^{-7}
Thalamus	1.98×10^{-4}	4.28×10^{-4}	1.51×10^{-4}	1.61×10^{-5}	3.26×10^{-5}
Thyroid	1.54×10^{-6}	1.55×10^{-6}	1.55×10^{-6}	1.87×10^{-7}	2.32×10^{-7}
White matter	2.94×10^{-5}	4.09×10^{-5}	2.72×10^{-5}	3.41×10^{-6}	6.03×10^{-6}

TABLE A7
S-Values for Listed Radionuclides with Spinal CSF as Source Region

Targets	S-value (mGy MBq^{-1} s^{-1})				
	^{11}C	^{15}O	^{18}F	^{99m}Tc	^{123}I
Caudate nucleus	2.24×10^{-6}	2.24×10^{-6}	2.24×10^{-6}	3.10×10^{-7}	3.74×10^{-7}
Cerebellum	3.96×10^{-6}	3.97×10^{-6}	3.96×10^{-6}	4.88×10^{-7}	6.12×10^{-7}
Cerebral cortex	2.50×10^{-6}	2.51×10^{-6}	2.50×10^{-6}	3.05×10^{-7}	3.88×10^{-7}
Eyes	1.22×10^{-6}	1.22×10^{-6}	1.22×10^{-6}	1.24×10^{-7}	1.53×10^{-7}
Lentiform nucleus	3.40×10^{-6}	3.41×10^{-6}	3.40×10^{-6}	4.60×10^{-7}	5.60×10^{-7}
Skin in head	2.48×10^{-6}	2.49×10^{-6}	2.49×10^{-6}	2.73×10^{-7}	3.52×10^{-7}
Skin in neck	7.67×10^{-6}	7.70×10^{-6}	7.68×10^{-6}	9.06×10^{-7}	1.19×10^{-6}
Skull	3.24×10^{-6}	3.90×10^{-6}	3.12×10^{-6}	5.59×10^{-7}	7.68×10^{-7}
Spinal column	2.46×10^{-4}	7.41×10^{-4}	1.43×10^{-4}	3.27×10^{-5}	5.90×10^{-5}
Spinal skeleton	9.86×10^{-5}	1.88×10^{-4}	8.06×10^{-5}	1.21×10^{-5}	2.76×10^{-5}
Thalamus	3.51×10^{-6}	3.52×10^{-6}	3.51×10^{-6}	5.16×10^{-7}	6.36×10^{-7}
Thyroid	7.83×10^{-6}	7.86×10^{-6}	7.85×10^{-6}	1.04×10^{-6}	1.33×10^{-6}
White matter	2.47×10^{-6}	2.48×10^{-6}	2.48×10^{-6}	3.11×10^{-7}	3.87×10^{-7}

TABLE A8
S-Values for Listed Radionuclides with Thalamus as Source Region

Targets	S-value (mGy MBq^{-1} s^{-1})				
	^{11}C	^{15}O	^{18}F	^{99m}Tc	^{123}I
Caudate nucleus	6.27×10^{-5}	6.79×10^{-5}	6.27×10^{-5}	8.10×10^{-6}	1.56×10^{-5}
Cerebellum	8.86×10^{-6}	8.89×10^{-6}	8.87×10^{-6}	1.20×10^{-6}	1.72×10^{-6}
Cerebral cortex	1.08×10^{-5}	1.08×10^{-5}	1.08×10^{-5}	1.46×10^{-6}	2.19×10^{-6}
Eyes	4.87×10^{-6}	4.88×10^{-6}	4.88×10^{-6}	5.77×10^{-7}	7.16×10^{-7}
Lentiform nucleus	1.98×10^{-4}	4.29×10^{-4}	1.50×10^{-4}	1.61×10^{-5}	3.26×10^{-5}
Skin in head	3.36×10^{-6}	3.37×10^{-6}	3.37×10^{-6}	3.85×10^{-7}	4.96×10^{-7}
Skin in neck	1.05×10^{-6}	1.06×10^{-6}	1.06×10^{-6}	1.06×10^{-7}	1.34×10^{-7}
Skull	6.99×10^{-6}	7.03×10^{-6}	7.00×10^{-6}	1.46×10^{-6}	2.19×10^{-6}
Spinal column	1.60×10^{-6}	1.61×10^{-6}	1.61×10^{-6}	2.15×10^{-7}	2.73×10^{-7}
Spinal skeleton	3.73×10^{-6}	3.75×10^{-6}	3.74×10^{-6}	7.77×10^{-7}	9.09×10^{-7}
Thalamus	1.02×10^{-2}	1.73×10^{-2}	7.09×10^{-3}	4.93×10^{-4}	9.02×10^{-4}
Thyroid	1.47×10^{-6}	1.47×10^{-6}	1.47×10^{-6}	1.71×10^{-7}	2.10×10^{-7}
White matter	3.08×10^{-5}	4.28×10^{-5}	2.84×10^{-5}	3.59×10^{-6}	6.31×10^{-6}

TABLE A9
S-Values for Listed Radionuclides with Third Ventricle as Source Region

Targets	S-value (mGy MBq^{-1} s^{-1})				
	^{11}C	^{15}O	^{18}F	^{99m}Tc	^{123}I
Caudate nucleus	4.66×10^{-5}	4.68×10^{-5}	4.67×10^{-5}	6.14×10^{-6}	1.12×10^{-5}
Cerebellum	9.09×10^{-6}	9.13×10^{-6}	9.11×10^{-6}	1.23×10^{-6}	1.78×10^{-6}
Cerebral cortex	1.09×10^{-5}	1.09×10^{-5}	1.09×10^{-5}	1.47×10^{-6}	2.21×10^{-6}
Eyes	4.88×10^{-6}	4.90×10^{-6}	4.89×10^{-6}	5.94×10^{-7}	7.34×10^{-7}
Lentiform nucleus	8.47×10^{-5}	8.51×10^{-5}	8.49×10^{-5}	1.08×10^{-5}	2.12×10^{-5}
Skin in head	3.37×10^{-6}	3.38×10^{-6}	3.38×10^{-6}	3.78×10^{-7}	4.86×10^{-7}
Skin in neck	1.05×10^{-6}	1.05×10^{-6}	1.05×10^{-6}	1.06×10^{-7}	1.33×10^{-7}
Skull	7.07×10^{-6}	7.11×10^{-6}	7.08×10^{-6}	1.47×10^{-6}	2.21×10^{-6}
Spinal column	1.73×10^{-6}	1.73×10^{-6}	1.73×10^{-6}	2.34×10^{-7}	2.90×10^{-7}
Spinal skeleton	3.81×10^{-6}	3.83×10^{-6}	3.82×10^{-6}	8.14×10^{-7}	9.56×10^{-7}
Thalamus	3.13×10^{-4}	5.96×10^{-4}	2.98×10^{-4}	3.75×10^{-5}	7.94×10^{-5}
Thyroid	1.45×10^{-6}	1.46×10^{-6}	1.45×10^{-6}	1.73×10^{-7}	2.12×10^{-7}
White matter	4.55×10^{-5}	8.98×10^{-5}	3.54×10^{-5}	3.93×10^{-6}	7.06×10^{-6}

TABLE A10
S-Values for Listed Radionuclides with White Matter as Source Region

Targets	S-value (mGy MBq^{-1} s^{-1})				
	^{11}C	^{15}O	^{18}F	^{99m}Tc	^{123}I
Caudate nucleus	3.32×10^{-5}	4.92×10^{-5}	3.00×10^{-5}	3.78×10^{-6}	6.79×10^{-6}
Cerebellum	7.74×10^{-6}	7.77×10^{-6}	7.75×10^{-6}	1.03×10^{-6}	1.57×10^{-6}
Cerebral cortex	1.52×10^{-5}	2.01×10^{-5}	1.42×10^{-5}	1.77×10^{-6}	3.00×10^{-6}
Eyes	5.41×10^{-6}	5.43×10^{-6}	5.42×10^{-6}	6.53×10^{-7}	8.30×10^{-7}
Lentiform nucleus	2.91×10^{-5}	4.06×10^{-5}	2.68×10^{-5}	3.40×10^{-6}	5.97×10^{-6}
Skin in head	4.01×10^{-6}	4.02×10^{-6}	4.02×10^{-6}	4.54×10^{-7}	6.18×10^{-7}
Skin in neck	8.32×10^{-7}	8.34×10^{-7}	8.34×10^{-7}	6.75×10^{-8}	8.87×10^{-8}
Skull	8.10×10^{-6}	8.14×10^{-6}	8.11×10^{-6}	1.53×10^{-6}	2.72×10^{-6}
Spinal column	1.16×10^{-6}	1.17×10^{-6}	1.17×10^{-6}	1.35×10^{-7}	1.71×10^{-7}
Spinal skeleton	2.47×10^{-6}	2.49×10^{-6}	2.48×10^{-6}	4.86×10^{-7}	5.68×10^{-7}
Thalamus	2.91×10^{-5}	4.06×10^{-5}	2.67×10^{-5}	3.60×10^{-6}	6.29×10^{-6}
Thyroid	1.04×10^{-6}	1.04×10^{-6}	1.04×10^{-6}	1.13×10^{-7}	1.41×10^{-7}
White matter	1.21×10^{-4}	2.00×10^{-4}	8.88×10^{-5}	7.38×10^{-6}	1.34×10^{-5}

TABLE A11
S-Values for Listed Radionuclides with Thyroid as Source Region

Targets	S-Value (mGy MBq^{-1} s^{-1})		
	^{99m}Tc	^{123}I	^{131}I
Caudate nucleus	1.28×10^{-7}	1.56×10^{-7}	4.19×10^{-7}
Cerebellum	9.08×10^{-8}	1.12×10^{-7}	3.11×10^{-7}
Cerebral cortex	9.51×10^{-8}	1.18×10^{-7}	3.24×10^{-7}
Eyes	1.14×10^{-7}	1.46×10^{-7}	4.55×10^{-7}
Lentiform nucleus	1.82×10^{-7}	2.22×10^{-7}	5.68×10^{-7}
Skin in head	1.19×10^{-7}	1.58×10^{-7}	4.06×10^{-7}
Skin in neck	1.68×10^{-6}	2.84×10^{-6}	5.22×10^{-6}
Skull	1.62×10^{-7}	1.87×10^{-7}	3.65×10^{-7}
Spinal column	4.60×10^{-7}	5.83×10^{-7}	1.29×10^{-6}
Spinal skeleton	1.62×10^{-6}	2.22×10^{-6}	3.21×10^{-6}
Thalamus	1.91×10^{-7}	2.28×10^{-7}	5.17×10^{-7}
Thyroid	1.58×10^{-4}	2.92×10^{-4}	1.61×10^{-3}
White matter	1.13×10^{-7}	1.39×10^{-7}	3.66×10^{-7}

ACKNOWLEDGMENTS

This work was supported by the U.S. Department of Energy, Office of Health and Environmental Research, grant DE-FG03-94ER61846 with the Texas A&M Research Foundation and the University of Florida.

REFERENCES

1. London ED. *Imaging drug action in the brain*. Boca Raton: CRC Press; 1993.
2. Saha GB, Macintyre WJ, Go RT. Radiopharmaceuticals for brain imaging. *Semin Nucl Med* 1994;24:324–349.
3. Poston JW. Research on the experimental verification of dosimetry calculations. Research proposal. DOE Report DE-AS05-790EV10248; June 1984.
4. Snyder WS, Ford MR, Warner GG, Fisher HL. Estimates of absorbed fractions for monoenergetic photon sources uniformly distributed in various organs of a heterogeneous phantom. MIRD pamphlet no. 5. *J Nucl Med* 1969;10(suppl):5–52.
5. Snyder WS, Ford MR, Warner GG. Estimates of specific absorbed fractions for photons sources uniformly distributed in various organs of a heterogeneous phantom. *MIRD pamphlet no. 5, revised*. New York: Society of Nuclear Medicine; 1978.
6. Cristy M. Mathematical phantoms representing children of various ages for use in estimates of internal dose. Tennessee: Oak Ridge National Laboratory Rep. ORNL/NUREG/TM-367; 1980.
7. Cristy M, Eckerman KF. Specific absorbed fractions of energy at various ages from internal photons sources. I. Methods. Tennessee: Oak Ridge National Laboratory Rep. ORNL/NUREG/TM-8381: Vol. 1; 1987.
8. Eckerman KF, Cristy M, Warner GG. Dosimetric evaluation of brain scanning agents. *Proceedings of the Third International Radiopharmaceutical Dosimetry Symposium*; 1980:527–540.
9. International Commission of Radiological Protection. *Report of the task group on reference man*. Oxford: Pergamon Press; ICRP Publication 23; 1975.
10. Johansson L, Nosslin B. Dosimetry of intrathecally administration radiopharmaceuticals. *Proceedings of the Fifth International Radiopharmaceutical Dosimetry Symposium*: 1992:188–201.
11. Blinkov SM, Glezer II. The human brain in figures and tables. New York: Plenum Press; 1968.
12. Kurepina MM. Structure and phylogenetic development of the thalamus in primates. *Arkh Biol Nauk* 1938;49:116–131.
13. Harman PJ, Carpenter MV. Volumetric comparisons of the basal ganglia of various primates including man. *J Comp Neurol* 1950;93:125–139.
14. Tompsett DH, Last RJ. Casts of the cerebral ventricles. *Br J Surg* 1953;40:525–543.
15. Murtagh FR, Schnitzlein HN. *Imaging anatomy of the head and spine*. Baltimore: Urban and Schwarzenberg; 1985:1–200.
16. Nelson WR, Hirayama, Rogers H. The EGS4 code system. Stanford University Linear Accelerator Center, Report 265; 1985.
17. Bouchet LG. A new head and brain dosimetry model. Master's thesis, Texas A&M University, 1995.